BBA - Biomembranes 1860 (2018) 2272–2280

Contents lists available at ScienceDirect

BBA - Biomembranes

journal homepage: www.elsevier.com/locate/bbamem

A DIE responsive NIR-fluorescent cell membrane probe

Dan Wu[a], Shane Cheung[a], Gonzalo Sampedro[a], Zhi-Long Chen[b], Ronan A. Cahill[c], Donal F. O'Shea[a,*]

[a] Department of Chemistry, RCSI, 123 St Stephen's Green, Dublin 2, Ireland
[b] Department of Pharmaceutical Science & Technology, College of Chemistry and Biology, Donghua University, Shanghai 201620, China
[c] Department of Surgery, Mater Misericordiae University Hospital (MMUH), School of Medicine, University College Dublin, Dublin, Ireland

ARTICLE INFO

Keywords:
NIR-fluorophore
Disaggregation-induced emission
Plasma membrane
Live cell
Fixed cell
NIR-fluorescence microscopy

ABSTRACT

It is challenging to achieve selective off to on modulation of the emissive state of a fluorophore within a complex and heterogeneous cellular environment. Herein we show that the dis-assembly of a non-fluorescent aggregate to produce individual fluorescent molecules, termed disaggregation induced emission (DIE), can be utilised to achieve this goal with an amphiphilic BF_2-azadipyrromethene (NIR-AZA) probe. Optical near-infrared properties of the NIR-AZA probe used in this study include absorption and emission maxima at 700 and 726 nm respectively when in the emissive non-aggregated state. Key to the success of the probe is the bis-sulfonic acid substitution of the NIR-AZA fluorophore, which is atypical for membrane probes as it does not contain zwitterionic lipid substituents. The aggregation/disaggregation properties of the NIR-fluorophore have been investigated in model surfactant and synthetic liposomal systems and shown to be emissive responsive to both. Real-time live cell imaging experiments in HeLa Kyoto and MC3T3 cells showed a rapid switch on of emission specific to the plasma membrane of viable and apoptotic cells attributable to a disaggregation-induced emission of the probe. Image analysis software confirmed localisation of fluorescence to the plasma membrane. Cell membrane staining was also effective for formaldehyde fixed cells, with staining possible either before or after fixation. This study adds new and important findings to recent developments of DIE responsive probes and further applications of this controllable emission-switching event are anticipated.

1. Introduction

Fluorescence based laboratory techniques remain a mainstay approach for investigating bio-molecular interactions in cellular, tissue and in vivo systems [1]. Yet interference from non-specific background fluorescence outside the imaging region of interest (ROI) remains a major limitation of non-specific diffusing molecular fluorophores [2]. This lack of selectivity often requires a time delay to allow non-selective fluorophore to redistribute naturally away from the ROI or to be cleared experimentally by washing. This can severely limit the acquisition of image data to individual time points, without the possibility of continuous data acquisition. A recognized solution to enhance ROI to background signal ratio is not to rely on selectively positioning the probe but rather have the probe turn on selectively in the ROI in a predictable manner. Molecular fluorescent probes can offer a solution to this drawback as they have the potential to transform from continuous light beacons to ones that can alternate between dark and emissive states in response to localized biological stimuli [3]. This can facilitate continuous real-time imaging, rather than image capture at static time points, eliminating the need to manipulate cells or the experimental removal of excess fluorophore. Such probes allow researchers to progress from picture images to movies, which are richer in data, allowing for more informed scientific interpretation of complex biological events [4]. Commonly used mechanisms to establish a non-fluorescent state of a fluorophore rely upon the covalent attachment of an analyte specific receptor group which quenches the excited state through photoinduced electron transfer (PeT) or internal charge transfer (ICT) processes [5]. These have shown remarkable successes for biologically relevant molecular analytes. Yet the principals surrounding off/on fluorescence responsive interactions between supramolecular self-assemblies of probes and biological surfaces and membranes remain relatively unexplored. We have recently turned our attention to developing useful emission responsive probes that selectively recognize biological and synthetic surfaces rather than specific molecular analytes [6].

The majority of fluorescence imaging has historically been conducted using the 400–600 nm spectral range, but more recently the advantages of lower energy near-infrared (NIR) spectral region

* Corresponding author.
E-mail address: donalfoshea@rcsi.ie (D.F. O'Shea).

https://doi.org/10.1016/j.bbamem.2018.09.006
Received 7 May 2018; Received in revised form 30 August 2018; Accepted 6 September 2018
Available online 08 September 2018
0005-2736/ © 2018 Elsevier B.V. All rights reserved.

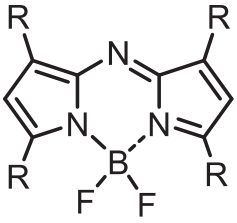

Fig. 1. BF_2-azadipyrromethene (NIR-AZA) fluorophore class.

(700–800 nm) are being increasingly recognized [7]. Specifically, NIR probes can be more suitable for real-time continuous imaging as they have the optimal wavelengths for minimal light induced toxicity, and their maximum penetration of light through body tissue means that they are directly translatable to in vivo use [8,9]. We have focused our efforts on the BF_2-azadipyrromethene (NIR-AZA) fluorophore class as they have excellent photophysical characteristics including substituent determined emission maxima between 675 and 800 nm, high quantum yields and exceptional photostability (Fig. 1) [10]. These properties have allowed them to be utilised for both in vitro live cell and in vivo imaging, while offering the potential for clinical applications in fluorescence guided surgery [11,12]. Previous work has shown that their emissions can be made responsive through PeT and ICT mechanisms [13]. In this report, we have investigated the use of molecular aggregation and disaggregation of a NIR-AZA probe to elicit the desired bio-controlled fluorescence switching.

Primarily, two styles of aggregation-controlled emission exist. The first, termed aggregate induced emission (AIE), is the self-assembly of non-emissive fluorophores into fluorescent aggregates (Fig. 2A). The second is directionally opposite, is called disaggregation induced emission (DIE) and is the dis-assembly of a non-fluorescent aggregate producing individual fluorescent molecules (Fig. 2B) [14–17]. Both approaches provide the required basis for a bio-responsive off to on switch. However, the major challenge lies in selectively switching the probe on not only in the controlled environment of a spectroscopy cuvette but also in more complex live cell experiments.

In this report, a specific NIR-AZA fluorophore has been investigated for real-time plasma membrane imaging using a DIE to provide a membrane responsive emission. Robust plasma membrane staining is needed for numerous research uses such as automated cell identification and status, translocation assays and the studying of plasma membrane dynamics [18]. Cell plasma membranes play significant roles in numerous biological events including cell division, endocytosis, exocytosis, signal transduction, exosome formation and release and apoptosis, yet few NIR-fluorescent membrane staining reagents have been designed. Cell mask deep red (647/666) and DiR (750/788) are the more commonly used longer wavelength stains, though the limitations of each have been well recognized [19–21]. As the plasma membrane provides the boundary between the cell and the surrounding

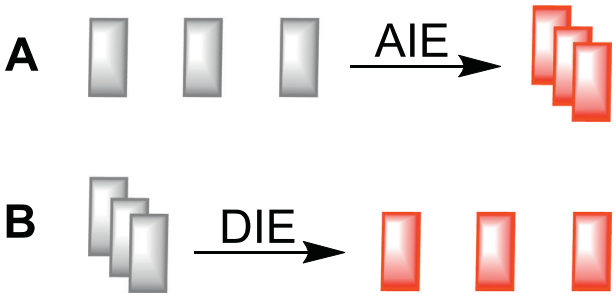

Fig. 2. Simplified schematic for AIE and DIE aggregate controlled emissions. Rectangle (molecular fluorophore); grey colour (non-fluorescent state); red colour (fluorescent state). (For interpretation of the references to colour in this figure legend, the reader is referred to the web version of this article.)

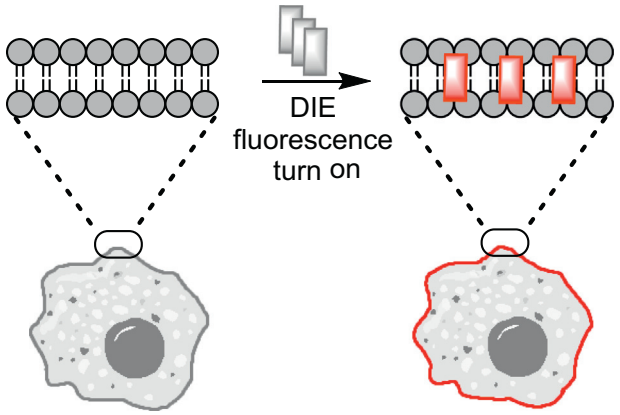

Fig. 3. Simplified schematic showing membrane induced DIE for real-time imaging. Rectangle (molecular fluorophore), grey colour (non-fluorescent), red colour (fluorescent). (For interpretation of the references to colour in this figure legend, the reader is referred to the web version of this article.)

microenvironment, it offers the opportunity to develop DIE based probes that are responsive to the interface between them. Conceptually, self-aggregation would provide a reservoir of non-emissive probe in cell media, which upon cell membrane induced dis-aggregation would generate an emissive form of the probe (Fig. 3). In this scenario, background noise is minimized and assuming the DIE is selective for the membrane bilayer, then real-time imaging becomes possible.

The most commonly utilised structural design features for membrane probes are the inclusion of ammonium salt, zwitterionic lipid or peptide substituents to facilitate favourable probe/membrane electrostatic interactions [18,20]. These substituent/membrane interactions should anchor the probe within the bilayer for a sufficient length of time for experimental image capture. For this work, we reasoned that such substituents would not be required and identified the NIR-AZA **1** as a potential DIE probe as it is a readily dispersible, non-emissive aggregate in water, while in organic media is strongly fluorescent (Fig. 4A). The DIE design of **1** was based on its amphiphilic properties, consisting of a hydrophobic fluorophore substituted on one face with two sulfonic acid groups linked via an aliphatic spacer. The role of sulfonic acid groups is to impart sufficient water solubility for ease of use and to act as a membrane anchor, by ionic association, with the ammonium component of membrane phospholipids (Fig. 4B) [22,23]. The hydrophobic face of **1** would be expected to induce self-aggregation in aqueous media and quench the emission as a result, though the overall amphiphilic balance of the molecule would permit its efficient cell membrane uptake. It was anticipated that upon membrane uptake, resulting in a change to a more lipophilic microenvironment, the emission from **1** would turn on due to dis-aggregation. Our expectation was that the membrane anchoring of two sulfonic acid groups would be sufficient to hold the fluorophore within the plasma membrane for a sufficient length of time (30–60 min) for dynamic imaging. Following which, internalization would occur as part of the normal membrane recycling processes that give rise to intracellular vesicles. Once internalized, the vesicles would be stained allowing their visualisation through the normal cellular pathways.

2. Materials and methods

2.1. Materials and solutions

All chemicals and liposomal mixture were purchased from Sigma-Aldrich and used without further purification. All reaction solvents were freshly purified and degassed before use. HPLC grade water used for experimental and analytical procedures.

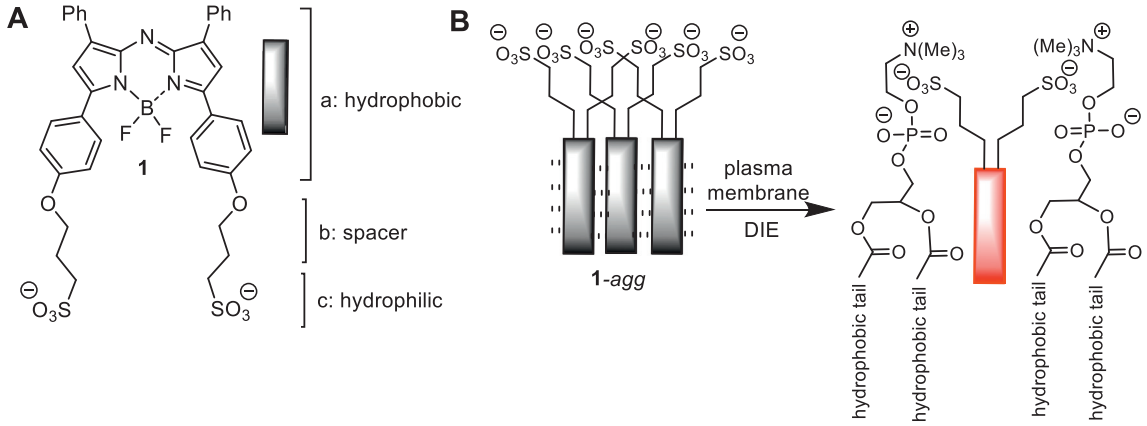

Fig. 4. (A) Amphiphilic NIR-AZA probe **1**. (B) Simplified schematic showing representation of membrane DIE activation of aggregated probe **1**. Fluorescence off (grey), fluorescence on (red), (only half of membrane bi-layer shown for clarity). (For interpretation of the references to colour in this figure legend, the reader is referred to the web version of this article.)

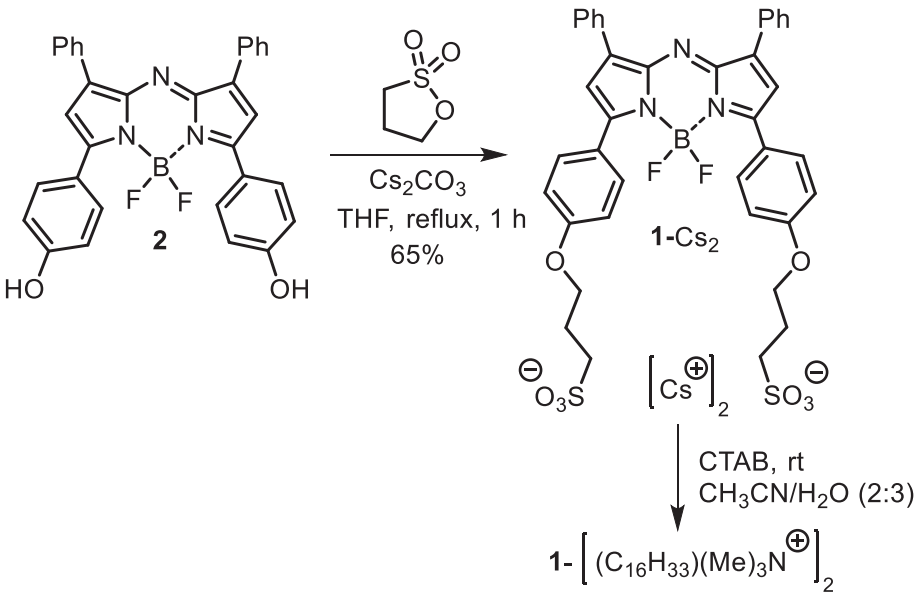

Scheme 1. Synthesis of NIR-AZA **1** as cesium and hexadecyltrimethylammonium (CTA) salts.

Table 1
Photophysical characteristics of **1**.

Entry	1	solvent	λ abs(nm)	fwhm(nm)	λ em(nm)[a]	Φ_{flu}[b]
1	**1**-Cs_2	MeOH	686	68	716	0.18
2	**1**-CTA_2	MeOH	686	73	717	0.17
3	**1**-Cs_2	H_2O	692	110	719	< 0.01
4	**1**-Cs_2	DMEM	698	109	724	< 0.01
5	**1**-CTA_2	H_2O	717	108	726	< 0.01
6	**1**-CTA_2	DMEM	718	112	725	< 0.01
7	**1**-Cs_2	H_2O/CTAB[c]	701	83	727	0.013
8	**1**-Cs_2	DMEM/CTAB[d]	700	74	726	0.18

[a] Excitation at 630 nm.
[b] 5,5-Difluoro-3,7-bis(4-methoxyphenyl)-1,9-diphenyl-5*H*-4l4,5l4-dipyrrolo [1,2-c:2′,1′-f][1,3,5,2]triazaborinine used as standard [26].
[c] 0.5 mM CTAB.
[d] 1 mM CTAB.

2.2. Methods

Column chromatography was performed using Sephadex G-25 column eluting with HPLC grade water. The pure fractions were identified by reverse phase HPLC with YMC triart phenyl column (size: 150 × 4.6 mm I.D, particle size: S-5 μm) at detector wavelength of 650 nm. ^{1}H NMR, ^{13}C NMR and ^{19}F NMR spectra were recorded on a Bruker spectrometer at 400 MHz, 100 MHz and 376 MHz respectively, and calibrated using residual non-deuterated solvent as an internal reference. Chemical shifts are reported in parts-per-million (ppm). HRMS-ESI mass spectra were acquired using a microTOF-Q spectrometer interfaced to a Dionex UltiMate 3000 LC in positive and negative modes as required. UV–Vis spectra were recorded using a Varian Cary 50 Scan UV–visible spectrophotometer. Fluorescence emission spectra were recorded using a Varian Cary Eclipse fluorescence spectrophotometer. All UV–Vis and fluorescence emission spectral plots were produced by using SigmaPlot 8 software.

2.3. Synthesis of probe *1*

2.3.1. BF_2 chelate of 3-(4-(3-phenyl-2-((3-phenyl-5-(4-(3-sulfonatopropoxy) phenyl)-1H-pyrrol-2-yl)imino)-2H-pyrrol-5-yl)phenoxy)propane-1-sulfonate (*1*-Cs_2) [24]

A solution of **2** [25] (100 mg, 0.19 mmol) in dry THF (2 mL) was treated with Cs_2CO_3 (309 mg, 0.95 mmol) and stirred at 0 °C under N_2 for 15 min. 1,3-Propanesultone (59 mg, 0.48 mmol) was added and the suspension was warmed to rt and then heated under reflux for 1 h. The

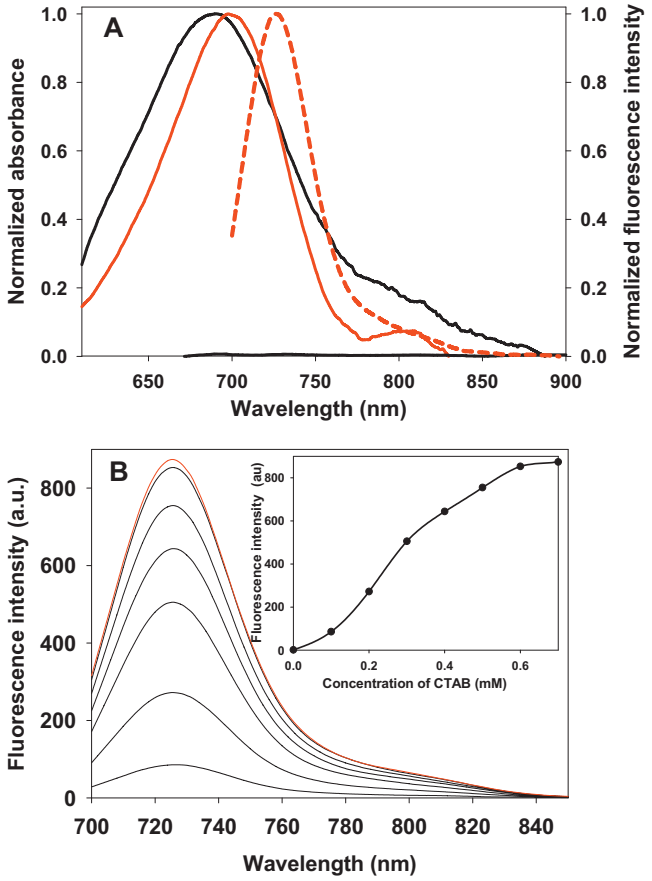

Fig. 5. Spectra of **1**-Cs_2 in DMEM and responses to CTAB. (A) Absorption (solid lines) and emission (dashed lines) spectra of **1**-Cs_2 in DMEM (black traces) and in DMEM/0.6 M CTAB (red trace). (B) Fluorescence responsive titration of **1** with CTAB in DMEM. (For interpretation of the references to colour in this figure legend, the reader is referred to the web version of this article.)

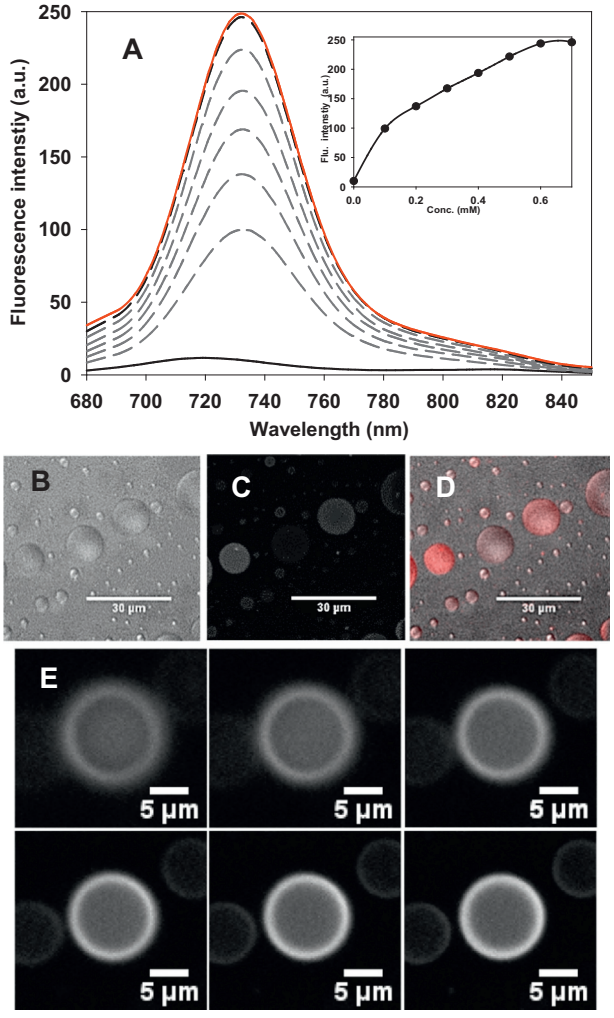

Fig. 6. DIE fluorescence switch on in liposomes. (A) Increasing emission intensity with sequential addition of liposomes to **1**. (B) DIC image of liposomes. (C) NIR-fluorescence (showing in white for clarity) image of liposomes. (D) Overlay of NIR-fluorescence (red colour) and DIC images. (E) Z-stack analysis of a single liposome (fluorescence shown in white). (For interpretation of the references to colour in this figure legend, the reader is referred to the web version of this article.)

mixture was cooled to rt, the precipitate filtered and the isolated solid washed with cold DCM (30 mL). Purification by Sephadex G-25 column eluting with HPLC grade water, combined fractions were freeze dried to give the product **1**-Cs_2 as a dark green solid (95 mg, 65%), mp > 250 °C. ^{1}H NMR (400 MHz, DMSO-d_6) δ 8.23–8.13 (m, 8H), 7.62 (s, 2H), 7.58–7.43 (m, 6H), 7.13 (d, J = 9.1 Hz, 4H), 4.23 (t, J = 6.5 Hz, 4H), 2.63 (t, J = 6.5 Hz, 4H), 2.12–2.03 (m, 4H). ^{13}C NMR (100 MHz, DMSO-d_6 + 5% $CDCl_3$): δ 161.9, 157.8, 144.9, 142.4, 138.3, 132.3, 130.0, 129.6, 129.2, 123.5, 120.3, 115.4, 67.6, 48.2, 25.6 ppm. ^{19}F NMR (376 MHz, DMSO-d_6): δ −130.43 (q, J = 32.2 Hz, F) ppm. HRMS (ESI): calcd. for $C_{38}H_{33}BF_2N_3O_8S_2$ $[M\text{-}H]^-$ 772.1770; found 772.1757.

2.3.2. *Conversion of **1**-Cs_2 into **1**-CTA_2*

A solution of **1**-Cs_2 (20 mg, 0.019 mmol) in acetonitrile/water (5 mL, 2:3) was treated with CTAB (2.2 eq, 16 mg, 0.043 mmol) and stirred at rt for 20 h. Solvent was removed by freeze drying and the crude product partitioned between $CHCl_3$ (30 mL) and H_2O (30 mL). The organic phase was washed with H_2O (3 × 30 mL), dried and evaporated to give a green solid (8.27 mg, 30%), mp 121–123 °C. ^{1}H NMR (400 MHz, $CDCl_3$) δ: 8.00–7.80 (m, 8H), 7.44–7.23 (m, 6H), 7.08–6.80 (m, 6H), 4.34 (t, J = 5.9 Hz, 4H), 3.08–3.05 (m, 4H), 3.01–2.93 (m, 4H), 2.85 (s, 18H), 2.23 (t, J = 6.4 Hz, 4H), 1.42–1.35 (m, 4H), 1.31–1.14 (m, 52H), 0.79 (t, J = 6.9 Hz, 6H) ppm.

2.4. *Preparation and spectroscopic measurements of liposomes*

Liposomes were composed from the commercial available mixture of cholesterol, L-α-phosphatidylcholine and stearylamine, in a 1:7:2 μmol ratio. To prepare the liposomes, HPLC grade water (1 mL) was added into the vial containing the components listed above at room temperature and mix by vortex for 30 s. This resulted in a milky suspension of liposomes which were used within 24 h. For emission titration studies, sequential aliquots of liposome stock solution were added to an aqueous solution of **1**-Cs_2 (5 μM) (exc. 660 nm) and the fluorescence spectrum recorded immediately after each addition.

2.5. *Microscopy apparatus*

Images were acquired on an Olympus IX73 epi-fluorescent microscope fitted and Andor iXon Ultra 888 EMCCD using a 60×/1.42 oil PlanApo objective (Olympus) and MetaMorph (Molecular Devices, v7.8.1) image acquisition software. NIR fluorescence channel: excitation was provided by a 640 (14) nm solid state light source, emission was collected using a 705/72 nm bandpass filter. Objective used 60×/1.42 oil PlanApo objective (Olympus). Z-scans were acquired with a z-steps of 0.5 μm or 1.0 μm.

2.5.1. *Image analysis and processing*

Deconvolution was performed using the Classic Maximum

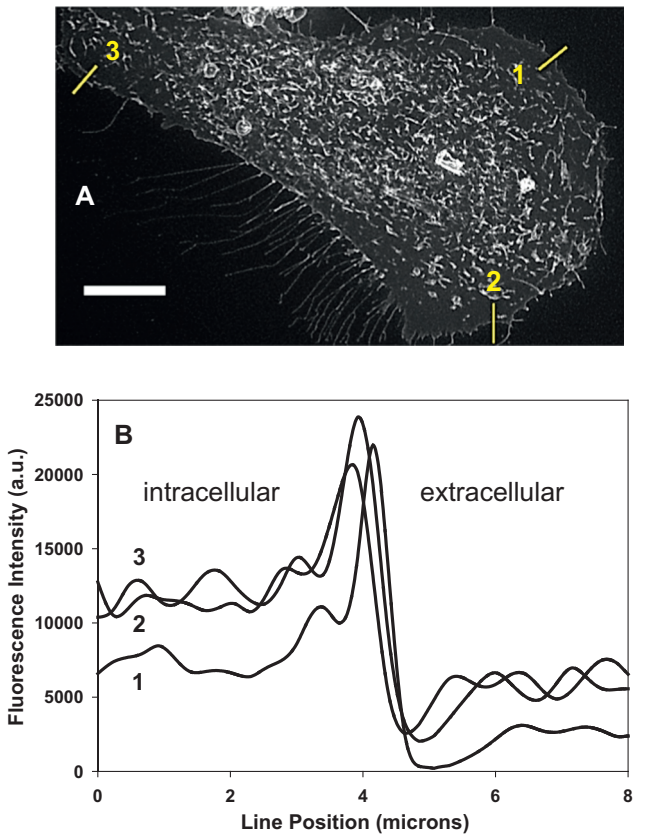

Fig. 7. (A) HeLa cell after 10 min incubation with **1** showing plasma membrane and filopodia staining, scale bar 20 μm. (B) Fluorescence line profile analysis at three different positions, marked 1–3 in panel A, showing selective staining of the plasma membrane.

Likelihood Estimation algorithm in Huygen's Professional (SVI, v15.10) software. Additional processing such as the creation of montages, videos, look up tables (LUT), and scaling was performed using FIJI software.

2.5.2. Line profiles

The line drawing tool function in FIJI software was used to draw a line ROI centred at the visible edge of the plasma membrane. The "Plot Profile" function was used to measure the fluorescence intensity at each pixel under the line. Fluorescence intensity values were plotted versus microns along the line (microns were selected for the x-axis to show where intensity changes were in relation to the line-ROI).

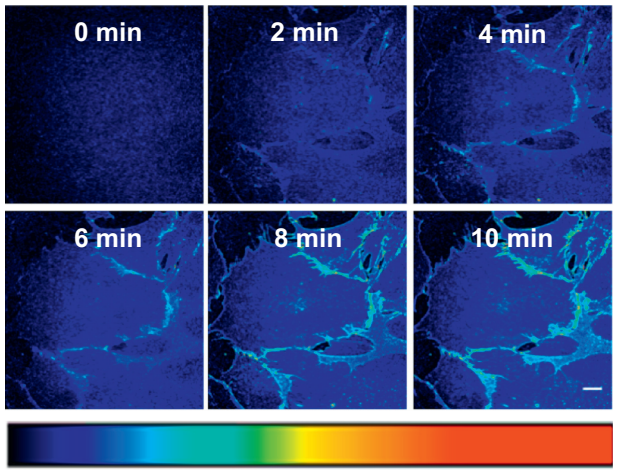

Fig. 9. Heat map showing increasing membrane fluorescence over 10 min in MC3T3 cells, scale bar 20 μm. For additional independent experiment, see Movie S8.

2.5.3. Heatmap images

The heatmap images and movies were created by applying the Royal look up table (LUT) in FIJI software to grayscale images and videos to make the range of fluorescence intensity found in the image correlate to a specific colour where black was the lowest value of the dynamic range, and red was the highest value of the dynamic range.

2.6. Cell imaging

2.6.1. Cell culture

HeLa Kyoto were cultured in DMEM supplemented with 10% FBS, 1% L-Glutamate, 1% Penicillin-streptomycin. MC3T3 cell were cultured in α-MEM supplemented with 10% FBS, 1% L-Glutamate, 1% Penicillin-streptomycin. Cells fixed with 2% para-formaldehyde (PFA) solutions at rt.

2.6.2. Live cell imaging protocol

10,000 HeLa Kyoto or MC3T3 mouse osteoblast cells were seeded on an eight well Ibidi chamber slide at a density of 1×10^4 cells per well 24 h before imaging. Slides placed on the microscope stage, and a field of view containing a suitable selection of cells was selected. Cell media was removed from the well and replaced with 200 μL of cell media containing **1** (5 μM) and the imaging protocol was started. Images acquired at either 10 s or 1 min intervals. Z-stacks were created using sufficient 1 μm or 0.5 μm separated optical slices to record the entire cell volume.

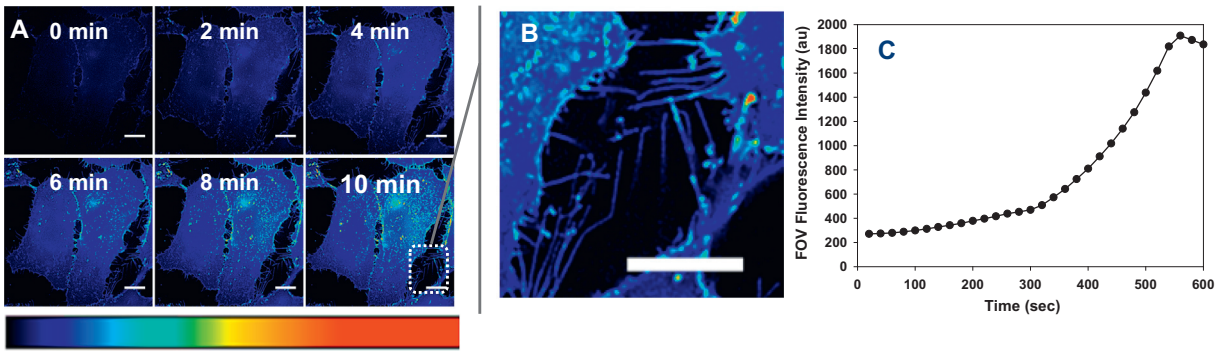

Fig. 8. Heat map showing increasing membrane fluorescence over 10 min in HeLa cells, scale bar 20 μm. (A) Heat map showing fluorescence intensity change over time. (B) Expanded section at 10 min time point showing filopodia in motion. (C) Plot of FOV fluorescence intensity over time.

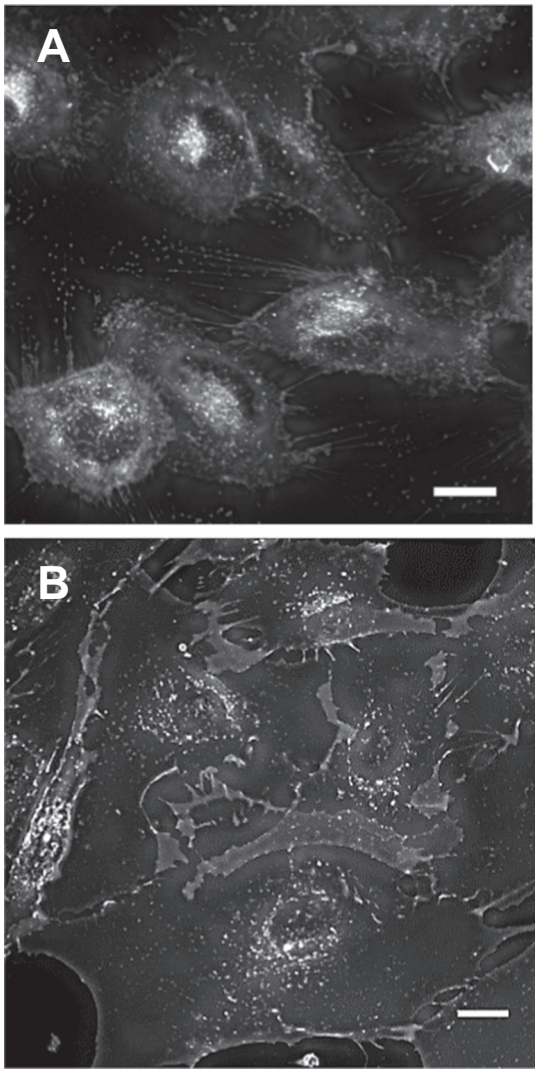

Fig. 10. Live cell imaging following 90 min incubation with **1**. (A) HeLa cells (B) MC3T3 cells showing both plasma membrane and intracellular vesicle staining. Scale bar 20 μm.

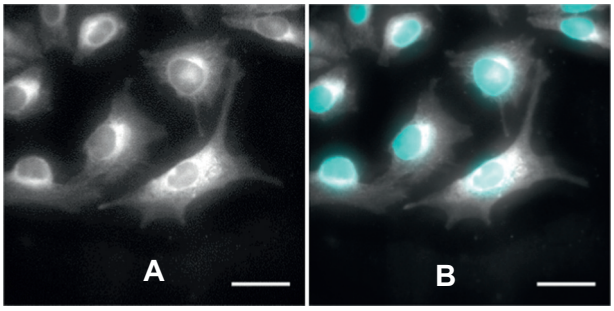

Fig. 11. Live cells treated with **1**, fixed with PFA, Hoescht33342 and imaged. (A) NIR-emission image of **1**. (B) Overlay of emissions from **1** and Hoescht33342. Scale bar 40 μM.

*2.6.3. Incubation of live cells with **1** followed by PFA fixation*

HeLa Kyoto cells were seeded at 1×10^4 cells per well on an eight well chamber slide (Ibidi) and allowed to proliferate for 24 h at 5.0% CO_2 and 37 °C. Media was replaced by fresh media and the cells treated with **1** (5 μM, PBS) and incubated at 37 °C for 20 min. The media was removed from wells and cells washed three times with PBS and fixed with 2% PFA for 5 min at rt. PFA was removed and cells and washed

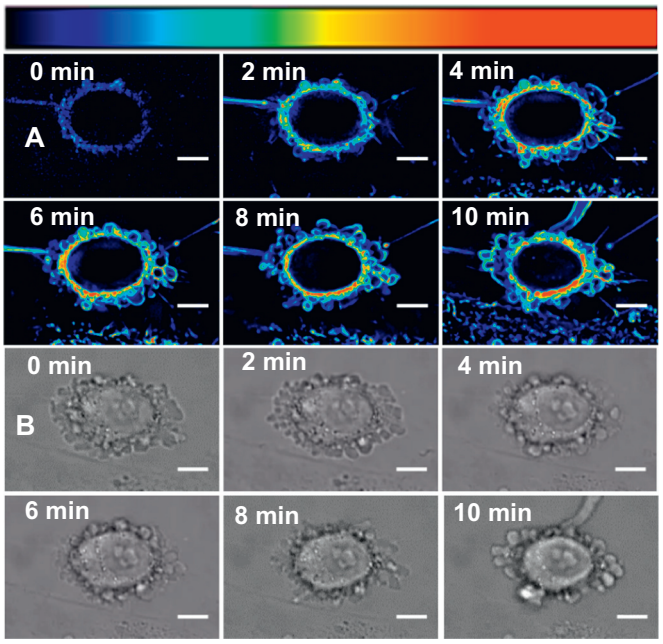

Fig. 12. Real-time image of apoptotic cell with **1**. (A) NIR-fluorescence images (B) DIC images taken over 10 min. Scale bar 20 μM.

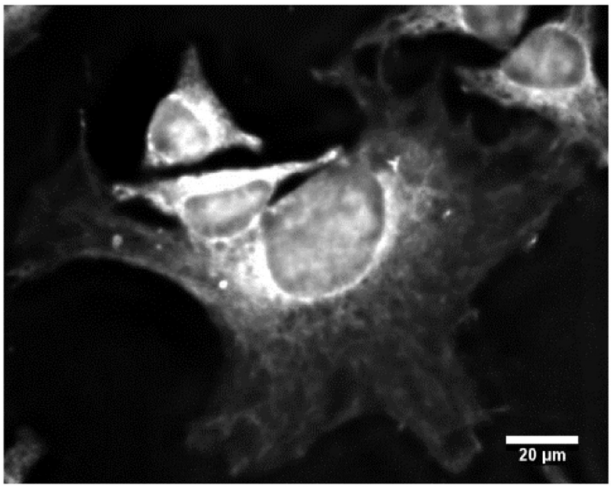

Fig. 13. Imaging of PFA fixed cells following treatment with **1**. NIR-fluorescence shown in white for clarity. Scale bar 20 μM.

three times with PBS. Nuclei were stained with Hoescht33342 (5 μg/mL) in PBS.

2.6.4. Fixed cell imaging

HeLa Kyoto cells were seeded at 1×10^4 cells per well on an eight well chamber slide (Ibidi) and allowed to proliferate for 24 h at 5.0% CO_2 and 37 °C. The media removed from wells, cells were washed three times with PBS and treated with 2% PFA for 5 min at rt PFA was removed and cells washed three times with PBS. Cells then were treated with **1** (5 μM, PBS) for 20 min and washed three times with PBS. Nuclei were stained with Hoescht33342 (5 μg/mL) in PBS.

2.6.5. Fixed cell imaging following permeabilising with Triton X100 (TX100)

HeLa Kyoto cells were seeded at 1×10^4 cells per well on an eight well chamber slide (Ibidi) and allowed to proliferate for 24 h at 5.0% CO_2 and 37 °C. The media removed from wells, cells were washed three times with PBS and treated with 2% PFA for 5 min at rt PFA was

removed and cells washed three times with PBS. Cells were treated with TX100 solution (0.1%, PBS) for 5 min at rt. The TX100 solution removed and cells washed three times with PBS. Cells then were treated with **1** (5 μM, PBS) for 20 min and washed three times with PBS. Nuclei were stained with Hoescht33342 (5 μg/mL) in PBS.

3. Results and discussion

Synthesis of probe **1** was achieved from the known substrate **2** with some refinement of a previously reported method (Scheme 1) [24]. Reaction of **2** with 1,3-propane sultone in THF under reflux for 1 h using $CsCO_3$ as base gave the di-cesium salt **1**-Cs_2 as a dark coloured solid in 65% yield. NMR and MS analytical data was consistent with the product. The inorganic counter-ion could be exchanged to its di-cetyl trimethylammonium (CTA) salt by treatment with the quaternary ammonium surfactant cetyltrimethylammonium bromide (CTAB) in acetonitrile/water at rt (Scheme 1).

In order to mimic the aqueous extracellular medium and hydrophobic environment of a membrane bilayer, the spectroscopic characterization of **1** was investigated using MeOH, water and Dulbecco's modified Eagle's medium (DMEM). As anticipated, **1** showed good spectral characteristics in methanol as either its cesium or ammonium salt with absorption and emission maxima at 686 and 717(± 1) nm respectively and a fluorescence quantum yield of 0.18 (Table 1, entries 1 and 2, Fig. S1). In contrast, solutions of **1** as its cesium salt in water or DMEM showed broadened and bathochromically shifted absorbance bands (λ_{max} 692 nm, 689 nm respectively) and very weak emissions (Table 1 entries 3, 4, Fig. 5A). A similar trend was observed for the d-CTA salt derivative with the absorption bands showing more pronounced bathochromatic shifts and very weak emissions (Table 1 entries 5, 6, Fig. S2). These results revealed that, as anticipated, fluorophore aggregation induces quenching of the emission and the changing of the counter-ion from an inorganic to organic salt, in it, did not significantly change the spectroscopic properties.

As changing the counter-ion from Cs to CTA was insufficient to produce an emission, the response of **1** to micelle formation using CTAB as a model surfactant was next investigated. This investigation was carried out by titration of aqueous solutions of **1**-Cs_2 with CTAB, which has a reported critical micelle concentration (CMC) range of 0.5–1.0 mM [27]. In pure water, it was found that little change in emission occurred below 0.3 mM CTAB, but above this concentration, the emission dramatically increased, reaching a maximum intensity at 0.5 mM (Fig. S3). Conducting the same experiment in the more complex aqueous solvent system of DMEM also showed a large enhancement of emission intensity, which reached a maximum at 0.6 mM concentration of CTAB (Fig. 5B). The presence of aggregated **1** was confirmed by dynamic light scattering (DLS) measurements of aqueous solutions which showed particles of size approximately 230 nm. After allowing the solution to stand for 3 h the particle size distribution became more complex as a distribution of smaller and larger aggregates are formed (Fig. S4).

These results show that a supramolecular fluorescence response of **1** to a CTAB micellar environment is possible but the changing of the cation alone, from Cs to CTA, does not. These results serve to illustrate how a predictable DIE event may be exploitable to selectively generate a fluorescence output from **1**.

As changes to emission intensity due to pH differences are known to complicate cell image interpretation the emission spectra of DMEM/CTAB **1** solutions were recorded at pH values ranging of 5 to 8 and, encouragingly, no changes were observed (Fig. S5).

Next, the ability of **1**-Cs_2 to NIR-fluorescent label a synthetic liposomal model was examined. Liposomes were made from L-α-phosphatidylcholine, stearylamine and cholesterol (7:2:1) as previously described [28]. To test the ability of liposomes to effect a DIE on **1**, equal amounts of vesicle were added sequentially to **1** (5 μM, water) and an emission spectrum recorded immediately after each addition. Pleasingly, emission intensities incrementally increased upon each addition showing an effective liposomal induced DIE (Fig. 6A and inset). Next, liposomes stained with **1** were viewed using widefield microscopy in both differential interference contrast (DIC) and NIR-fluorescence imaging modes. Individual and overlaid images confirmed that the liposomes were fluorescent, (Fig. 6B–D), and 3D Z-stack analysis of liposomes showed the strongest fluorescence signal was from the interfacial liposome layer (Fig. 6E, Movies S1 and S2).

With the DIE responsive nature of **1** established, the potential for translation of this concept to real-time plasma membrane imaging was next investigated. For this study the human cervical and mouse osteoblast cell lines HeLa Kyoto and MC3T3 respectively were chosen as representative examples for investigation. For real-time DIE responsive experiments, chamber slide seeded cells were placed in a widefield microscope surrounded by an incubator to maintain the temperature at 37 °C and CO_2 at 5%, following which an imaging FOV containing viable cells was chosen. The cells were treated with **1** (5 μM) and time-lapse fluorescence images were acquired for 10 min with 1 min intervals between image acquisitions (Movie S3). In both cell lines, a rapid, within 2 min, switch on of fluorescence specific to the plasma membrane was observed which could be attributed to the association of **1** with the membrane bilayer. The fluorescence intensity continued to increase across the entire membrane over time, with many distinctive cellular filopodia protrusions readily observed after 10 min (Fig. 7A).

Using ImageJ software, ROI lines were drawn at three distinct cell positions (numbered 1–3 in Fig. 7A) such that the centre of the line was at a visible edge of the plasma membrane with half inside and half outside of the cell. Using the Plot Profile software function, the fluorescence intensity at each pixel along the lines was measured with the data shown in Fig. 7B as a plot of line position versus fluorescence intensity. This clearly shows that background fluorescence in the extracellular media is low with a large increase in intensity measurable at the membrane and a significantly lower intensity beyond this point within the cell body. This analysis nicely illustrates that a selective DIE of **1** can provide the contrast necessary for real-time image capture. Also, z-stack image analysis of the cell at 10 min was consistent with membrane staining (Movie S4). Next, increasing the rate of image capture to every 10 s for a selection of viable HeLa cells showed that the onset of DIE within the plasma membrane was very rapid with the entire membrane visible within 4 min with excellent background contrast. Representative time points in Fig. 8A are shown as a heat map of fluorescence intensity increasing rapidly over time. Plotting fluorescence intensity changes in the cell FOV over time illustrated a highly effective DIE of **1** taking place within 600 s (Fig. 8C). Combining the thirty individual images taken over the first 10 min time-period into a movie format allowed the visualisation of filopodia in motion and pairs of filopodia making contact from neighbouring cells (Fig. 8B, Movies S5 and S6).

A very similar DIE profile was recorded for experiments using MC3T3 cells with weak membrane localized fluorescence observable almost immediately after the addition of **1** which quickly increased, allowing clear cell outlines to be visible by 4 min (Fig. 9, Movie S7).

Imaging both cell lines after a longer 90 min incubation time showed that while cell membrane remained stained, internalization of probe **1** had also occurred with distinct punctuate pattern of bright spots indicative of vesicle staining (Fig. 10). 3D Z-stack images through the cytoplasm confirmed that the vesicles were intracellular (Movies S9 and S10).

While inevitably, cell fixation results in loss of the finer structural membrane elements identifiable in live cell imaging at times it is required for some high-throughput assay formats [29]. Pleasingly, incubation of HeLa cells with **1** for 20 min followed by washing and room temperature fixing with 2% paraformaldehyde (PFA) and nuclear staining with Hoescht33342 gave excellent images clearly showing cell membrane outlines (Fig. 11 and see Fig. S6 for a wider FOV). This shows that **1** is compatible with aldehyde fixation methods and the loss

of image quality is relatively small (see Movie S11 for z-stack images).

Apoptosis, or programmed cell death, is vital for the homeostatic regulation of cellular populations with dysfunctional cell death attributable to diseases such as cancer and neurodegeneration. As such, it is advantageous to be able to detect and image this process with the identification of apoptotic cells within a live cell population being an important feature of several assays [30]. As the DIE of **1** is the result of membrane interaction we reasoned that this should also apply to cells undergoing apoptosis. Experimentally, this was investigated by first identifying and focusing on a cell with notable apoptotic morphology using DIC microscopy. Immediately following the addition of **1**, both NIR-fluorescence and DIC imaging commenced and was continued for a 10 min time-period. Pleasingly, an effective DIE of **1** was induced by the apoptotic cell membrane which was seen to become NIR-emissive within 60 s and increased in intensity for the following 10 min (Fig. 12A, Movie S12 for black and white version see Fig. S7, Movie S13). The real-time imaging allowed dynamic visualisation of the formation of membrane blebs, microtubule spikes and apoptopodia as confirmed by comparison with the DIC images (Fig. 12B, Movie S14).

Finally, **1** was tested for its ability to DIE stain cells post PFA fixation with and without the use of a membrane permeabilising buffer solution. Experimentally, a PBS solution of **1** (5 μM) was added at room temperature to formaldehyde fixed cells for 20 min, the cells were washed with PBS and treated with Hoescht33342 to stain nuclei. Microscopy imaging showed an effective dual colour cell staining had been achieved (Fig. 13, see Fig. S8 for wider FOV). Imaging results were again positive showing the cell membrane outline and intracellular features, which were confirmed by z-stack analysis (Movie S15).

Fixed cell staining protocols often involve the use of several different labels including immunofluorescence labelling that require the use of membrane permeabilising agents. Post-PFA fixation cell permeabilization is required for immunostaining with primary and secondary antibodies, to allow the antibody access to the intracellular proteins. This separate permeabilization step use surfactants, such as Triton X-100 (TX100), which by default disrupt the cell membrane [31]. The fixed cell staining protocol was repeated as described above but cells were also treated with a 0.1% TX100 solution and washed immediately prior to addition of **1**. Imaging showed that cells were effectively stained though a reduction in the overall contrast of the cytoplasm with less definition of cell features was notable (Fig. S9). This is presumably due to the action of the surfactant on cell membranes. Taken together, the results of fixed cell imaging clearly show the potential of DIE staining using **1** and that it may be useful for a wide range of cell biology studies.

4. Conclusion

Employment of a controlled disaggregation induced emission strategy has allowed the development of a new class of NIR-fluorescence membrane probe. Dis-assembly of the fluorophore aggregate occurs upon interaction with cell membranes, generating an emissive form of the probe. The membrane selective off to on switching of the emission allows visualisation of dynamic cellular events in real-time, as the bulk of the fluorophore remains in a non-fluorescent dark state. The probe design is advantageous, as it does not employ expensive zwiterionic lipid substituents to realize the imaging goals. The amphiphilic nature of the probe is achieved with bis-sulfonic acid substituents, which are synthetically straightforward to introduce. The rationale for using an amphiphilic probe was to provide an aggregation-quenched emission form in bulk media, which upon association with the membrane bilayer would result in conversion to an emissive disaggregated state.

The NIR-probe showed a supramolecular fluorescence response to micellar CTAB and effectively labelled a synthetic liposomal model with emission maximum at 726 nm. In live cell experiments using HeLa Kyoto and MC3T3 cell the dynamic DIE response of **1** was visualised in real-time. The switch on of fluorescence, specific to the plasma membrane, was observable within seconds, and the increasing fluorescence intensity was monitored over time. ImageJ software analysis of image date confirmed localisation of fluorescence selectively to the plasma membrane. Rapid acquisition of image data allowed real-time visualisation of cell-cell contacts through pairs of filopodia. Live cell imaging was also possible for cells undergoing apoptosis. Additionally treatment of fixed cells with **1**, without the need of permeabilization agents, was an effective means of staining cells in a procedurally efficient manner. Ongoing studies include the translation of DIE controlled NIR-imaging to in vivo use with applications directed towards fluorescence-guided surgery.

Supplementary data to this article can be found online at https://doi.org/10.1016/j.bbamem.2018.09.006.

Transparency document

The Transparency document associated with this article can be found, in online version.

Acknowledgements

DOS gratefully acknowledges Science Foundation Ireland grant number 17/TIDA/4936 for financial support.

DOS declares the following competing financial interest. Patents have been filed on BF_2-azadipyrromethene based NIR fluorophores (EP2493898 and US8907107) in which he has a financial interest.

References

[1] K.M. Dean, A.E. Palmer, Advances in fluorescence labelling strategies for dynamic cellular imaging, Nat. Chem. Biol. 10 (2014) 512–523.
[2] J.C. Hsiang, A.E. Jablonski, R.M. Dickson, Optically modulated fluorescence bioimaging: visualizing obscured fluorophores in high background, Acc. Chem. Res. 47 (2014) 1545–1554.
[3] L. Yuan, W. Lin, K. Zheng, L. He, W. Huang, Far-red to near infrared analyte-responsive fluorescent probes based on organic fluorophore platforms for fluorescence imaging, Chem. Soc. Rev. 42 (2013) 622–661.
[4] S. Cheung, D. Wu, H. Daly, N. Busschaert, M. Morgunova, J. Simpson, D. Scholz, P.A. Gale, D.F. O'Shea, Real-time recording of the cellular effects of the anion transporter prodigiosin, Chem 4 (2018) 879–895.
[5] A.P. de Silva, H.Q.N. Gunaratne, T. Gunnlaugsson, A.J.M. Huxley, C.P. McCoy, J.T. Rademacher, T.E. Rice, et al., Chem. Rev. 97 (1997) 1515–1566.
[6] S. Cheung, D.F. O'Shea, Directed self-assembly of fluorescence responsive nanoparticles and their use for real-time surface and cellular imaging, Nat. Commun. 8 (2017) 1885.
[7] S. Wäldchen, J. Lehmann, T. Klein, S. van de Linde, M. Sauer, Light-induced cell damage in live cell super-resolution microscopy, Sci. Rep. 5 (2015) 15348.
[8] A.L. Vahrmeijer, M. Hutteman, J.R. van der Vorst, C.J.H. van de Velde, J.V. Frangioni, Image-guided cancer surgery using near-infrared fluorescence, Nat. Rev. Clin. Oncol. 10 (2013) 507–518.
[9] H. Kobayashi, M. Ogawa, R. Alford, P.L. Choyke, Y. Urano, New strategies for fluorescent probe design in medical diagnostic imaging, Chem. Rev. 110 (2010) 2620.
[10] Y. Ge, D.F. O'Shea, Azadipyrromethenes: from traditional dye chemistry to leading edge applications, Chem. Soc. Rev. 45 (2016) 3846–3864.
[11] M. Grossi, M. Morgunova, S. Cheung, D. Dimitri Scholz, E. Conroy, M. Terrile, A. Panarella, J.C. Simpson, W.M. Gallagher, D.F. O'Shea, Lysosome triggered near infra-red fluorescence; imaging of cellular trafficking processes in real-time, Nat. Commun. 7 (2016) 10855.
[12] H.C. Daly, G. Sampedro, C. Bon, D. Wu, G. Ismail, R.A. Cahill, D.F. O'Shea, BF_2-azadipyrromethene NIR-emissive fluorophores with research and clinical potential, Eur. J. Med. Chem. 135 (2017) 392–400.
[13] J. Killoran, D.F. O'Shea, Impact of a conformationally restricted receptor on the BF_2 chelated azadipyrromethene fluorosensing platform, Chem. Commun. (2006) 1503–1505.
[14] J. Mei, N.L.C. Leung, R.T.K. Kwok, J.W.Y. Lam, B.Z. Ben Zhong Tang, Aggregration-induced emission: together we shine, united we soar, Chem. Rev. 115 (2015) 11718.
[15] W. Zhang, C.Y.Y. Yu, R.T.K. Kwok, J.W.Y. Lam, B.Z. Tang, A photostable AIE luminogen with near infrared emission for monitoring morphological change of plasma membrane, J. Mater. Chem. B 6 (2018) 1501.
[16] D. Zhai, W. Xu, L. Zhangab, Y.T. Chang, The role of disaggregation in optical probe development, Chem. Soc. Rev. 43 (2014) 2402.
[17] X. Li, H. Jiang, Z. Luo, Y.-T. Chang, L. Zhang, Development of a disaggregation-induced emission probe for the detection of RecA inteins from *Mycobacterium*

tuberculosis, Chem. Commun. 52 (2016) 9086.
[18] C.W. Cairo, J.A. Key, C.M. Sadek, Fluorescent small-molecule probes of biochemistry at the plasma membrane, Curr. Opin. Chem. Biol. 14 (2010) 57.
[19] N.H. Revelo, D. Kamin, S. Truckenbrodt, A.B. Wong, K. Reuter-Jessen, E. Ellen Reisinger, T. Moser, S.O. Rizzoli, A new probe for super-resolution imaging of membranes elucidates trafficking pathways, J. Cell Biol. 205 (2014) 591.
[20] A.S. Klymchenko, R. Kreder, Fluorescent probes for lipid rafts: from model membranes to living cells, Chem. Biol. 21 (2014) 97.
[21] D.L. Marks, R. Bittman, R.E. Pagano, Use of bodipy-labeled sphingolipid and cholesterol analogs to examine membrane microdomains in cells, Histochem. Cell Biol. 130 (2008) 819.
[22] A. Cardone, F. Lopez, F. Affortunato, G. Busco, A.M. Hofer, R. Mallamaci, C. Martinelli, M. Colella, G.M. Farinola, An aryleneethynylene fluorophore for cell membrane staining, Biochim. Biophys. Acta 1818 (2012) 2808.
[23] O.A. Kucherak, S. Oncul, Z. Darwich, D.A. Yushchenko, Y. Arntz, P. Didier, Y. Mély, A.S. Klymchenko, Switchable nile red-based probe for cholesterol and lipid order at the outer leaflet of biomembranes, J. Am. Chem. Soc. 132 (2010) 4907.
[24] M. Tasior, J. Murtagh, D.O. Frimannsson, S.O. McDonnell, D.F. O'Shea, Water-solubilised BF_2-chelated azadipyrromethenes, Org. Biomol. Chem. 8 (2010) 522.
[25] J. Murtagh, D.O. Frimannsson, D.F. O'Shea, Azide conjugatable and pH responsive near-infrared fluorescent imaging probes, Org. Lett. 11 (2009) 5386.
[26] P. Batat, M. Cantuel, G. Jonusauskas, L. Scarpantonio, A. Palma, D.F. O'Shea, N.D. McClenaghan, BF_2-azadipyrromethenes: probing the excited-state dynamics of a NIR fluorophore and photodynamic therapy agent, J. Phys. Chem. A 115 (2011) 14034.
[27] D.B. Miraglia, J.L. Rodríguez, R.M. Minardi, P.C. Schulz, Critical micelle concentration and HLB of the sodium oleate–hexadecyltrimethylammonium bromide mixed system, J. Surfactant Deterg. 14 (2011) 401.
[28] P. Srinath, S.P. Vyas, P.V. Diwan, Preparation and pharmacodynamic evaluation of liposomes of indomethacin, Drug Dev. Ind. Pharm. 26 (2000) 313.
[29] A.J. Hobro, N.I. Smith, An evaluation of fixation methods: spatial and compositional cellular changes observed by Raman imaging, Vib. Spectrosc. 91 (2017) 31.
[30] J.C. Puigvert, H. de Bont, B. van de Water, E.H.J. Danen, High-throughput live cell imaging of apoptosis, Curr. Protoc. Cell Biol. 47 (1) (2010).
[31] M.C. Jamur, C. Oliver, Permeabilization of cell membranes, Methods Mol. Biol. 588 (2010) 63.